Robotica (2015) volume 33, pp. 1589–1608. © Cambridge University Press 2014
doi:10.1017/S0263574714000903

Adaptive source search in a gradient field

Xiaochen Zhang, Yi Sun* and Jizhong Xiao

Department of Electrical Engineering, The City College of New York, New York, USA

(Accepted March 11, 2014. First published online: April 25, 2014)

SUMMARY

Most existing source search algorithms suffer from a high travel cost, and few of them have been analyzed in performance in noisy environments where local basins are presented. In this paper, the theseus gradient search (TGS) is proposed to effectively overcome local basins in search. Analytical performances of TGS and the gradient ascend with correlated random walk (GACRW), which is a variant of correlated random walk, are derived and compared. A gradient field model is proposed as an analytical tool that makes it feasible to analyze the performances. The analytical average searching costs of GACRW and TGS are obtained for the first time for this class of algorithms in the environments with local basins. The costs, expressed as functions of searching space size, local basin size, and local basin number are confirmed by simulation results. The performances of GACRW, TGS, and two chemotaxis algorithms are compared in the gradient field and a scenario of indoor radio source search in a hallway driven by real data of signal strengths. The results illustrate that GACRW and TGS are robust to noisy gradients and are more competitive than the chemotaxis-based algorithms in real applications. Both analytical and simulation results indicate that in the presence of local basins, TGS almost always costs the lowest.

KEYWORDS: Biased and correlated random walk; Gradient ascend; Local maximum; Self-avoiding walk.

1. Introduction

Strategies behind search of sources have received attention in several disciplines. In the natural world, bacteria, insects, and animals have their own ways to find food, locate mates, pursue quarries, and avoid natural enemies. Laws behind these behaviors have been studied,[1,3,29,34] and then inspired a number of researches and applications in robotics community.[18,19,25,27,35] Specifically, robots can be dispatched to find hazardous chemical leaks[28] or radio sources in a wireless sensor network for the purpose of maintenance[32] and sweeping.[31]

Although the source types are distinct, most of these share a common property: the closer to the source, the higher the measured signal/density/luminance magnitude. Thus, a number of works published in the field use gradient ascent. However, in situations when gradients are very rugged, such hill climbing methods have a high chance to fail. Considering this, heuristic methods are used to guarantee success. Unfortunately, the time required by a heuristic method to ensure a significant probability of success usually exceeds the time required by an exhaustive search. Since a good algorithm should be fast and robust, alternative methods are proposed and studied. The E. coli algorithm[24] has been studied in the context of robotic source search by Russell *et al*.[26] This algorithm is one of the original chemotaxis methods. By comparing current measured concentrations or magnitudes with previous ones, a robot makes a decision on either moving along a straight path or making a random turn. A simplified chemotaxis is presented by Nurzaman *et al*.[20] The algorithm is similar to E. coli and has been studied in environments where magnitude measurements are not always available. An inspiring study states that a search can be performed with partial information and cues.[33] Another recent study has investigated on the kinematic state estimation and motion planing in an exponential map which has similar diffusion characteristics in moving.[21] The planar algorithm,

* Corresponding author. Email: ysun@ccny.cuny.edu.

https://doi.org/10.1017/S0263574714000903 Published online by Cambridge University Press

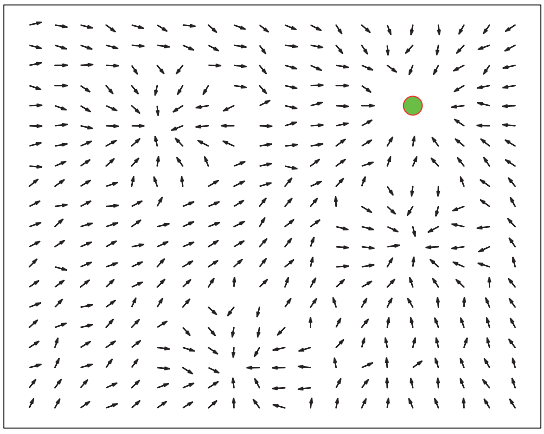


Fig. 1. Noisy gradients and three local basins in a source search. The green dot stands for the source and the dark arrows indicate the gradients.

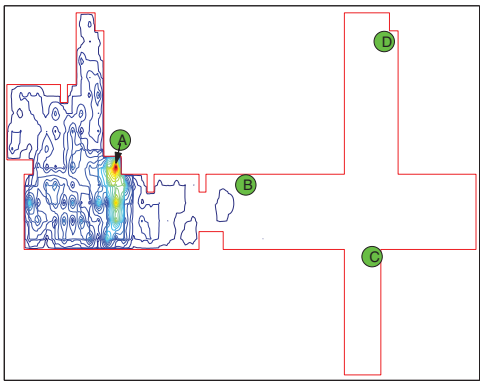


Fig. 2. An RSS contour map of radio source A in a hallway. The red lines stand for the wall edge; B, C, D are other sources.

taking advantage of zigzag movements and multiple magnitude meters, is studied in the context of underground chemical source localization.[10,26] A similar algorithm, using zigzag to guide a mobile robot to a chemical source, has been reported by Ishida *et al.*[13] The Hex-Path algorithm is believed to be a better choice with lower average travel cost compared with the E. coli and planar algorithms, but it has a risk of failure since it cannot distinguish between a local basin and the global basin.[26] Recently, navigations using multi-resolution algorithm have new breakthroughs in terms of robust complete coverage, which seamlessly integrates local and global navigations.[8,14,15] In our earlier studies, we proposed an adaptive gradient method which uses weighted gradients in a recent short period as the guide.[32] However, the algorithm itself cannot guarantee success. We have proposed an algorithm combining the gradient method with the self-avoiding walk that reduces the cost in noisy environments.[38] We have also proposed searching algorithms using the force field vector that leads fast map coverage.[36,37] All these works are under the condition that a reverse propagation model illustrating the correlation between distances and magnitudes is not an option; otherwise, a Bayes filter-based simultaneous localization can be applied.[30]

To the best of our knowledge, most results obtained by the related works are based on numerical simulations and laboratory experiments. Very limited work presents an analysis on algorithm performance with respect to the environment status. In general, a searching mobile robot has to face challenges as noisy gradients and local basins, as shown in Fig. 1. Noisy gradients indicate situations where gradients of magnitudes are more likely pointing to a position around the true source instead of exactly to it; while local basins indicate situations where gradients are always toward local maxima. These challenges are inevitable in practical scenarios. For example, Fig. 2 shows the contour map of received signal strength (RSS) distribution of a single wireless access node in a hallway. Fortunately, noisy gradients can be easily dealt with smoothing gradients using multiple

https://doi.org/10.1017/S0263574714000903 Published online by Cambridge University Press

readings; and local basins can be overcome by either heuristic methods,[6] random walks,[24] or arbitrary exhaustive methods.[38] Although all these methods can overcome local basins, it is more interesting to know how much travel cost will be spent for a given scenario.

In this paper, the focus of study is the local basins since noisy gradients are not a major difficulty in source search. The analytical average travel costs of gradient ascend with correlated random walk (GACRW) and theseus gradient search (TGS) in a gradient field are obtained. It is shown that TGS has a lower travel cost than GACRW when local basins are dense and large. The results are verified by numerical simulations. We also carry out simulations with real data in the context of radio source search. Comparisons show that (i) in the gradient field, where the local basins are highlighted, TGS has a lower travel cost than the other three methods except the cases that local basins are small and sparse; (ii) in a radio source search, where both types of challenges are presented, TGS also has a lower cost than the other three methods; (iii) GACRW is a wise choice in the case that the location information necessary for TGS is unavailable since GACRW has a lower travel cost than the two chemotaxis-based algorithms when both types of challenges are presented. Henceforth, the cost and travel costs are used alternatively while both of them stand for the average travel distance in search.

The rest of the paper is organized as follows. In Section 2, GACRW and TGS algorithms are presented; the gradient field and local basins are defined. In Section 3, the analytical travel costs in both algorithms are obtained. In Section 4, simulation results are presented. In Section 5, conclusions are drawn and future work is discussed.

2. Algorithms and Gradient Field

2.1. Gradient ascent with correlated random walk

Biased and correlated random walk (BCRW) contains consistent biases in the preferred directions with certain persistence.[7, 22, 23] We apply GACRW, which is essentially a BCRW in source search. In brief, a robot follows gradients when the projection of the previous movements on the latest gradient is positive, as in Algorithm 1.

Algorithm 1 GACRW

```
1: while undone do
2:    if the inner product of current gradient and previous motion is positive then
3:       move forward one step along current gradient.
4:    else
5:       make a rotation with an angle subject to N(0, σ^2) and move forward one step.
6:    end if
7:    end condition test.
8: end while
```

$N(0, \sigma^2)$ denotes the Gaussian distribution with mean 0 and standard deviation σ. Here σ is arbitrarily taken as $\frac{\pi}{2}$.

The algorithm comprises two phases: one is the gradient ascent; another is the correlated random walk (CRW). Apparently, in an ideal case, a robot using GACRW can reach the source with a cost equal to the Euclidean distance from the starting point to the source. However, if the robot is drawn to a local basin, it will arrive at the local maximum point first.

2.2. Theseus gradient search

Theseus gradient search is inspired by the self-avoiding walk. The robot's motion is planned on orthogonal grids. In other words, the original environment layout is understood as a scaled grid map by the robot. While searching, the robot prefers to go to unvisited points along a gradient. If gradients in a local area are always toward a local maximum point, the robot will behave as in an exhaustive search. TGS is robust and flexible: while gradients are toward the global maximum point, which is the source, the robot will approach it through its optimal path in the taxicab geometry; otherwise, the robot will perform the self-avoiding walk. One of the essential problems of self-avoiding walk is the

https://doi.org/10.1017/S0263574714000903 Published online by Cambridge University Press

high cost in high dimensions. However, the cost in two dimensions is $O(m^2)$, where m^2 stands for the area of the space. TGS algorithm is as follows.

Algorithm 2 TGS

```
Push the current robot location into the stack
while undone do
  if at least one neighbor of the stack top is unvisited then
    use unvisited neighbors as candidates;
    calculate inner products between the current gradient and the vectors heading to the candidates;
    move to the candidate with the largest inner product;
    push the selected candidate into the stack.
  else
    pop up the stack top.
  end if
  end condition test.
end while
```

Theseus gradient search integrates the robust exhaustive search with the optimal gradient ascent in searching. While TGS is efficient with almost every scenario, it has a chance to face the virtual wall dilemma. Briefly speaking, since the searching robot is unlikely to move to traveled positions, a robot's past path may block it from moving to the target in particular scenarios. In that case, the self-avoiding walk may prevent robot from moving toward the correct target. To deal with it, the study in Zhang *et al.*[38] provides a heuristic method in addition to TGS, which guarantees a success rate of over 0.95 in the search.

2.3. Gradient field

Most algorithms for source search, including GACRW and TGS, are discrete decision-making systems. At each step, a robot finds a direction along the gradient of magnitudes and makes a motion decision accordingly. The gradient at a point may be obtained using consecutive two measurements[2] or latest several measurements.[32] The path along which a search is performed can be irregular line segments,[20] zigzag,[27] or hex-path.[26] A lot of efforts have been made to alleviate the effect of noisy gradients, while much less for the local basins. Moreover, the local basins are the major challenges in source search. Thus, we intend to propose a scenario named gradient field where the local basins are highlighted.

Definition 1. **(Gradient field)** A gradient field is a square vector field where the gradient at any point always points to the unique maximum point.

Definition 2. **(Ideal searching space)** The ideal searching space is a gradient field with side length N at the center of which the global maximum point is located.

Definition 3. **(Local basin)** A local basin is a gradient field with side length m.

Definition 4. **(Searching space)** The searching space is an $N \times N$ ideal searching space with k local basins of size $m \times m$, as shown in Fig. 3.

In practice, the local basin side length m is related to the type of source, geometry layout of the environment, and diffusion time. Without loss of generality, the starting points of the robot and locations of local basins are regulated as follows.

Assumption 1. The searching robot with step length 1 starts from a random point in accordance with a uniform distribution.

Assumption 2. Local basins are located randomly in a searching space under the following conditions:
1. Local basins do not cover the global maximum point.
2. Local basins do not cover the areas outside the searching space.
3. Coordinates of local basin center (a, b) satisfy $\mathrm{mod}(a, m) = \mathrm{mod}(b, m) = 0$, where *mod* stands for a modulo operation.

https://doi.org/10.1017/S0263574714000903 Published online by Cambridge University Press

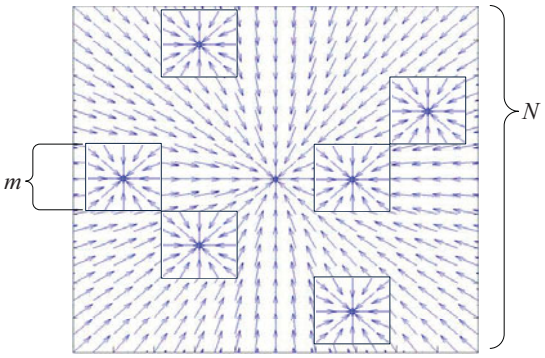


Fig. 3. An $N \times N$ searching space with six $m \times m$ local basins.

Obviously, the local basins are highlighted in the gradient field while the noisy gradients are omitted. Henceforth, the term *size* is used to represent the *side length* for convenience. A searching space is fully defined by searching space size N, local basin size m, and local basin number k, as shown in Fig. 3. For simplicity of calculation, N, m, and k are considered as integers. The average travel cost of each algorithm is investigated in the following section.

3. Travel Cost in the Gradient Field

3.1. Nomenclature

In order to facilitate the understanding of the following sections, we provide a brief nomenclature as follows:

ϕ	Probability density function of standard normal distribution.
Φ	Cumulative distribution function of standard normal distribution.
ω	Turning angle between consecutive steps.
θ_i	Turning angle at the ith step compared with the initial orientation.
σ	Standard deviation of the turning angle ω.
χ_f	Forward cost, see (b) in Section 3.2.1.
χ_b	Backward cost, see (b) in Section 3.2.1.
χ	Cost of reaching escape state, composed by forward cost and backward cost, see (b) in Section 3.2.1.
p_i, q_i, s_i	Transition probabilities to corresponding states, see (c) in Section 3.2.1.
e, f	Event of escaping a local basin and move to the next state respectively.
S_k^{GACRW}	Expected travel cost of a robot driven by GACRW in a searching space with k local basins.
S_k^{TGS}	Expected travel cost of a robot driven by TGS in a searching space with k local basins.
$\Re$	Additional cost, see Section 3.3.

https://doi.org/10.1017/S0263574714000903 Published online by Cambridge University Press

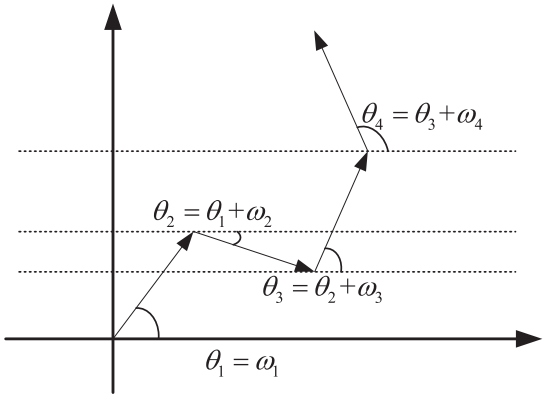


Fig. 4. Movements start from the origin. θ_i is the turning angle at the ith step compared with the initial orientation; ω_i is the turning angle at the ith step compared with that of the previous step.

3.2. Gradient ascent with correlated random walk

3.2.1. Cost of escaping a local basin. (a) Turning angle after n continuous CRW: When a robot is trapped in a local basin, the CRW phase is triggered. Before the robot escapes the local basin, it may go back to the center of local basin a few times. For example, after a few steps of CRW, the robot has a high chance to face back to the local basin center. In this case, the phase of gradient ascent draws the robot to the local basin center for one more time. Obviously, the escape consists of CRW, which drives the robot outward, and gradient ascent, which pulls the robot back to the local basin center.

The distribution of turning angle ω at each step can be approximated by a truncated Gaussian distribution:

$$f(\omega) = \frac{\frac{1}{\sigma}\phi(\frac{\omega}{\sigma})}{\Phi(\frac{\pi}{2\sigma}) - \Phi(-\frac{\pi}{2\sigma})}, \tag{1}$$

where ϕ denotes the probability density function of the standard normal distribution and Φ is its cumulative distribution function, σ denotes the standard deviation of the turning angle at each step.

Then for continuous n steps of CRW, the distribution of turning angle can be approximated by a Gaussian random variable with mean zero and variance $3n\pi^2/40$. This approximation is good enough to obtain the expected displacement as shown next.

(b) Expected displacement after n continuous CRW: A common way to find the expected displacement after n continuous CRW is to find the root of mean square displacement (MSD)[17] instead. The approximation is accurate when n is not a large number.[5] As shown in Fig. 4, $\theta_i = \theta_{i-1} + \omega_i = \sum_{j=1}^{i} \omega_j$.

Then the MSD after n continuous CRW can be written as:

$$\begin{aligned} E(R_n^2) &= E\left(n + \sum_{i \neq j} (\cos\theta_i \cos\theta_j + \sin\theta_i \sin\theta_j)\right) \\ &= n + E\left(\sum_{i \neq j} \cos(\theta_i - \theta_j)\right). \end{aligned} \tag{2}$$

Since $\theta_i - \theta_j = \sum_{l=\min(i,j)}^{\max(i,j)-1} \omega_l$, an approximated value of $E(R_n^2)$ can be obtained.

(c) Absorbing Markov chain in CRW: Before getting the overall cost, it is necessary to obtain the cost in escaping a single local basin. A difficulty is that the location of each step in CRW is not analytically tractable since it is not Markovian.[7,16] However, the moving average process[9] in the

https://doi.org/10.1017/S0263574714000903 Published online by Cambridge University Press

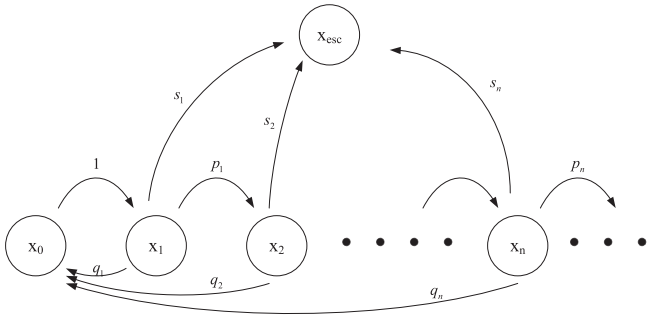


Fig. 5. Absorbing Markov chain of the CRW. At transient state x_i, the robot has a probability p_i to go to transient state x_{i+1}, q_i to go back to the initial state x_0, s_i to enter the absorbing state x_{esc}, and $p_i + q_i + s_i = 1$.

system can be viewed as a Markov chain if we define its states as follows:

$$\begin{aligned} x_0 &\equiv \{\text{Initial state: the robot is at the center ofthe local basin}\},\\ x_i &\equiv \{\text{Transient state } i\text{: the robot has launched } i \text{ consecutive CRW; } i \in \mathbb{N}^*\},\\ x_{\text{esc}} &\equiv \{\text{Absorbing state: the robot escapes thelocal basin}\}, \end{aligned}$$

where $\mathbb{N}^*$ denotes the nonzero natural number. Specifically, it is an absorbing Markov chain since the transition probability of the self-loop in x_{esc} is 1, as shown in Fig. 5. To enter the state x_{esc}, the cost χ can be resolved in two parts: the forward cost χ_f and the backward cost χ_b. The forward cost χ_f denotes the transition cost from state $i-1$ to i, $i \in \mathbb{N}^*$; the backward cost χ_b denotes the cost from state i to state 0,

$$\chi = \chi_f + \chi_b. \tag{3}$$

In an absorbing Markov chain, all states except the absorbing state are termed transient states. For computational convenience, we regard that a robot leaves a local basin if the displacement of robot from the center of local basin is no less than $m/\sqrt{\pi}$.

If we use e and f to denote the events of escaping a local basin and moving to the next state respectively, the corresponding transition probabilities of each state can be written as follows.

As shown in Fig. 5, the transition probabilities are: $s_0 = 0$, $p_0 = 0$; $s_1 = 1$ if $m \geq \pi^2$, otherwise $s_1 = 0$; $s_2 = \Pr(e_2|\bar{e}_1 f_1) = \frac{\Pr(e_2\bar{e}_1 f_1)}{\Pr(\bar{e}_1 f_1)}$, $p_2 = \Pr(\bar{e}_2|\bar{e}_1 f_1) \times \Pr(f_2|\bar{e}_1\bar{e}_2 f_1) = \Pr(\bar{e}_2 f_2|\bar{e}_1 f_1) = \frac{\Pr(\bar{e}_1 f_1\bar{e}_2 f_2)}{\Pr(\bar{e}_1 f_1)}$; $s_3 = \Pr(e_3|\bar{e}_1 f_1\bar{e}_2 f_2)$, $p_3 = \Pr(\bar{e}_3|\bar{e}_1 f_1\bar{e}_2 f_2) \times \Pr(f_3|\bar{e}_1 f_1\bar{e}_2 f_2\bar{e}_3) = \Pr(\bar{e}_3 f_3|\bar{e}_1 f_1\bar{e}_2 f_2) = \frac{\Pr(\bar{e}_1 f_1\bar{e}_2 f_2\bar{e}_3 f_3)}{\Pr(\bar{e}_1 f_1\bar{e}_2 f_2)}$.

All these probabilities can be written in multi-fold integral forms, such as:

$$\Pr(\bar{e}_1 f_1\bar{e}_2 f_2\bar{e}_3 f_3) = \int\limits_{\bar{e}_1 f_1\bar{e}_2 f_2\bar{e}_3 f_3}\int\int p(\omega_1)p(\omega_2)p(\omega_3)d\omega_1 d\omega_2 d\omega_3, \tag{4}$$

where p denotes the probability distribution function, $\omega_1, \omega_2, \omega_3$ denote the turning angle at step 1, 2, 3 respectively. $\bar{e}_1$ indicates $m \geq \pi^2$; $\bar{e}_2$ indicates $2 + \cos(\omega_2) \leq \frac{\pi^2}{m}$; $\bar{e}_3$ indicates $3 + 2[\cos(\omega_2) + \cos(\omega_3) + \cos(\omega_2 + \omega_3)] \leq \frac{\pi^2}{m}$. f_1 is always true; f_2 indicates $2k\pi - \frac{\pi}{2} \leq tg^{-1}(\frac{\sin(\omega_1)+\sin(\omega_1+\omega_2)}{\cos(\omega_1)+\cos(\omega_1+\omega_2)}) \leq 2k\pi + \frac{\pi}{2}$; f_3 indicates $2k\pi - \frac{\pi}{2} \leq tg^{-1}(\frac{\sin(\omega_1)+\sin(\omega_1+\omega_2)+\sin(\omega_1+\omega_2+\omega_3)}{\cos(\omega_1)+\cos(\omega_1+\omega_2)+\cos(\omega_1+\omega_2+\omega_3)}) \leq 2k\pi + \frac{\pi}{2}$, $k \in \mathbb{Z}$, where $\mathbb{Z}$ denotes the integer set.

To find the forward cost χ_f and backward cost χ_b, it is necessary to know the expected number of times the chain is in each state. For this purpose, we need to investigate on the transition matrix.

https://doi.org/10.1017/S0263574714000903 Published online by Cambridge University Press

We renumber the states of a transition matrix so that the transient states come first. If there are r absorbing states and t transient states, the transition matrix can be written in the canonical form[11] :

$$\mathbf{P} = \begin{pmatrix} \mathbf{Q} & \mathbf{R} \\ \mathbf{0} & \mathbf{I} \end{pmatrix}. \tag{5}$$

Here $\mathbf{I}$ is an r by r identity matrix, $\mathbf{0}$ is an r by t zero matrix, $\mathbf{Q}$ is a t by t matrix, and $\mathbf{R}$ is a nonzero t by r matrix. In the above absorbing Markov chain, $r = 1$ and t is infinity. $\mathbf{Q}$ and $\mathbf{R}$ are shown as follows,

$$\mathbf{Q} = \begin{pmatrix} 0 & 1 & 0 & 0 & \cdots & 0 \\ q_1 & 0 & p_1 & 0 & & 0 \\ q_2 & 0 & 0 & p_2 & & 0 \\ q_3 & 0 & 0 & 0 & & 0 \\ \vdots & & & & \ddots & \vdots \\ q_{t-1} & 0 & 0 & 0 & \cdots & 0 \end{pmatrix}, \tag{6}$$

$$\mathbf{R} = (0\ s_1\ s_2 \cdots s_{t-1})^T. \tag{7}$$

Recall, p_i denotes the transition probability from x_i to x_{i+1}, q_i denotes the transition probability from x_i to x_0, and s_i is the transition probability from x_i to x_{esc}. Due to the fact that $s_i \approx 1$ when i is large, t can be truncated as a large number instead of infinity. A fundamental matrix $\mathbf{N}$[11] can then be obtained as:

$$\mathbf{N} = (\mathbf{I} - \mathbf{Q})^{-1}. \tag{8}$$

The entry n_{ij} of $\mathbf{N}$ is the expected number of times that the chain is in x_j if it starts from x_i. A vector $\mathbf{L} = (n_{12}\ n_{13}\ n_{14} \cdots n_{1t})$ is picked up from the first row of N for the consequential calculation of travel cost.

Then the forward cost χ_f is:

$$\chi_f = \mathbf{L} \times c, \tag{9}$$

where c is a column vector of all 1's.

The backward cost is:

$$\chi_b = \mathbf{L} \times v, \tag{10}$$

where v is a column vector with entry $v_i = q_{i+1} \times \sqrt{E(R_i^2)}$. The expected cost of escaping a local basin can be found by (3).

However, as soon as a robot leaves a local basin, it has a probability to move back to the same local basin again. The probability depends on the position where the robot escapes. For example, if a robot escapes the leftmost local basin in the searching space in Fig. 3 from the left edge, it will immediately enter the same local basin again. When m is much larger than 1, possible escaping positions can be regarded as uniformly distributed on the corresponding local basin perimeter. Under Assumption 1 that local basins are square gradient fields, the probability of re-entering the same local basin is either 50% or 75%, depending on the location of the local basin. For example, if the local basin is located on the north of the center, the probability of re-entering the local basin is 75% since the robot leaves the local basin only if the escaping point is on the southern edge. On the other hand, if a local basin is located on the diagonal of the searching space, the re-entering probability is 50%.

3.2.2. Cost with $\boldsymbol{k}$ *local basins.* If there is no local basin in the searching space, the searching cost equals the distance between a starting point and the target. Regarding the searching space center as

https://doi.org/10.1017/S0263574714000903 Published online by Cambridge University Press

the origin in polar coordinates, the expected travel cost S_0^{GACRW} can be written as:

$$\begin{aligned} S_0^{\mathrm{GACRW}} &= \frac{8}{N^2}\int_0^{\frac{\pi}{4}}\int_0^{\frac{N}{2\cos\theta}} r \times r dr d\theta \\ &= \frac{N}{3}\int_0^{\frac{\pi}{4}} \sec^3\theta d\theta \\ &\approx 0.383\ N, \end{aligned} \tag{11}$$

where S denotes the cost in search, N denotes the size of the searching space, the superscript in S_0^{GACRW} indicates the name of algorithm, and the subscript 0 indicates that zero local basin is presented.

When k local basins are presented, a robot starting from a random point will meet α local basins on average, where $0 < \alpha < k$. The searching cost S_k^{GACRW} can be obtained by adding all the cost of escaping local basins on S_0^{GACRW}, where the subscript k in S_k^{GACRW} indicates that k local basins are presented. If a robot starts from a random point, the probability that the robot accesses a local basin can be written as:

$$\begin{aligned} P &= \frac{8m}{N^2(N-2m)^2} \times \int_0^{\frac{\pi}{4}}\int_{\frac{m}{2\cos\theta}}^{\frac{N}{2\cos\theta}-\frac{N}{2\cos\theta}} r^2(\cos\theta+\sin\theta)drd\theta \\ &= \frac{8m}{N^2(N-2m)^2} \times \frac{(N-2m)(N^2+m^2-mN)}{16} \\ &= \frac{m(N^2+m^2-mN)}{2N^2(N-2m)}, \end{aligned} \tag{12}$$

where m denotes the size of a local basin.

Thus, the number of local basins encountered by a searching robot is $\alpha \approx k \times P$. Recall that as soon as a robot leaves a local basin, it has a probability of either 50% or 75% to re-enter the same local basin right away. Furthermore, for the probability of 50%, the expected visiting time is $1 + \sum_{i=1}^{\infty}(1/2)^i = 2$; for the probability of 75%, the expected visiting time is $1 + \sum_{i=1}^{\infty}(3/4)^i = 4$. The probabilities are decided by the locations of local basins. By taking the repetitive counts into consideration, the total number of times that local basins are escaped is obtained as:

$$H = \frac{2N+6m}{N+m} \times kP. \tag{13}$$

Therefore, the searching cost S_k^{GACRW} is

$$S_k^{\mathrm{GACRW}} = S_0^{\mathrm{GACRW}} + H\chi. \tag{14}$$

3.3. Theseus gradient search

3.3.1. Cost with a local basin. The cost of escaping a single local basin using TGS is denoted as $g(m)$, which approximately equals to the local basin area m^2. When no local basin is presented, the expected cost S_0^{TGS} can be written as:

$$\begin{aligned} S_0^{\mathrm{TGS}} &= \frac{1}{N^2}\int\int_G (||x|| + ||y||)dxdy \\ &= \frac{1}{N^2}\int_{-\frac{N}{2}}^{\frac{N}{2}}\int_{-\frac{N}{2}}^{\frac{N}{2}} (||x|| + ||y||)dxdy \\ &= \frac{N}{2}, \end{aligned} \tag{15}$$

https://doi.org/10.1017/S0263574714000903 Published online by Cambridge University Press

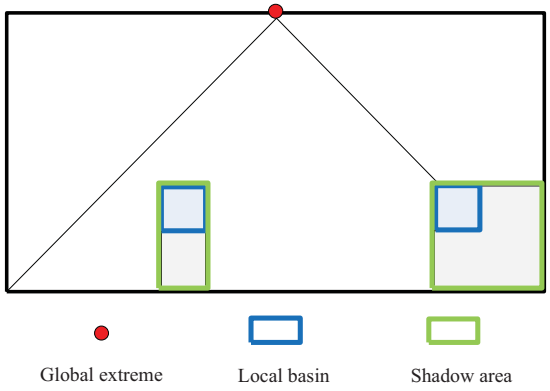


Fig. 6. Two cases of local basins with their shadow areas.

where S denotes the cost in search, G denotes the searching space, and N denotes the size of the searching space.

When presented in the searching space, local basins may trap the robot. A point is in shadow area F_i if the path to the global maximum point intersects the ith local basin. For example, Fig. 6 shows the global maximum point, two local basins, and their shadow areas.

When the searching space has one local basin, the expected cost S_1^{TGS} can be written as:

$$\begin{aligned} S_1^{\mathrm{TGS}} &= \frac{1}{N^2}\left[\int\int_F (||x|| + ||y|| + g(m))dxdy + \int\int_{G-F} (||x|| + ||y||)dxdy\right] \\ &= \frac{1}{N^2}\left[\int\int_F g(m)dxdy + \int\int_G (||x|| + ||y||)dxdy\right] \\ &= \frac{g(m)}{N^2}\int\int_F dxdy + S_0^{\mathrm{TGS}} \\ &= \Re + S_0^{\mathrm{TGS}}, \end{aligned} \tag{16}$$

where N denotes the size of the searching space, m denotes the size of local basins, and the subscript 1 indicates the number of local basins that appeared in the searching space.

Obviously, the additional cost $\Re = \frac{g(m)}{N^2}\int\int_F dxdy$ is proportional to the expected area of the shadow area $E(F) = \int\int_F dxdy$. Considering that the shadow area may occur in one out of the two forms in Fig. 6, an approximation of $E(F)$ can be written as follows:

$$\begin{aligned} E(F) \approx \frac{8}{N(N-2m)}\Bigg(& m\int_{\frac{m}{2}}^{\frac{N-m}{2}}\int_0^{x-\frac{m}{2}} \left(\frac{N}{2} - \frac{m}{2} - x\right)dydx \\ & + \int_{\frac{m}{2}}^{\frac{N-m}{2}}\int_{x-\frac{m}{2}}^{x} \left(\frac{N}{2} + \frac{m}{2} - x\right)\left(\frac{N}{2} + \frac{m}{2} - y\right)dydx\Bigg) \end{aligned}$$

https://doi.org/10.1017/S0263574714000903 Published online by Cambridge University Press

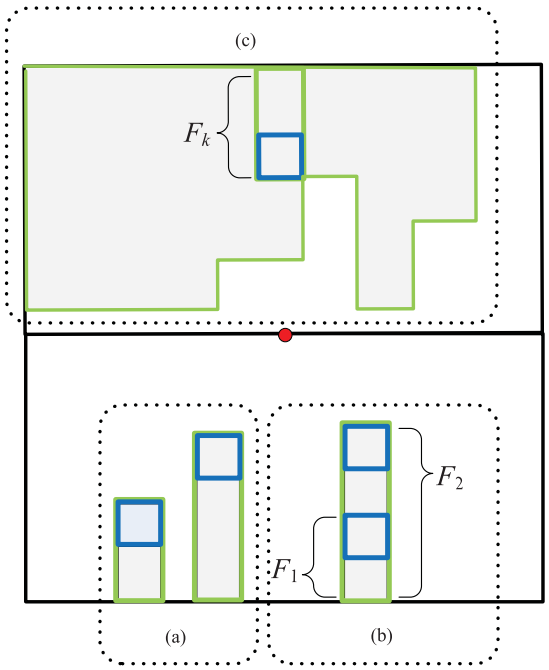


Fig. 7. (a) Two separated local basins; (b) two local basins with overlapping shadow areas; (c) adding the kth local basin to a searching space with $k-1$ local basins.

$$= \frac{8}{N(N-2m)}\left(\frac{m(N-2m)(N^2-8m^2+8mN)}{48} + \frac{m(N-2m)(4N^2+22m^2+11mN)}{192}\right)$$
$$= \frac{m(8N^2-10m^2+43mN)}{24N}. \tag{17}$$

3.3.2. Cost with two local basins. When two local basins are presented in the searching space, the cost S_2^{TGS} cannot be found directly since the locations of local basins are unpredictable.

Case 1

When the two shadow areas are not overlapped, i.e. $F_1 \cap F_2 = \varnothing$ as in Fig. 7(a), the cost can be directly written as:

$$S_{2.1}^{\mathrm{TGS}} \approx \frac{1}{N^2}\left[\int\int_F (||x||+||y||+g(m))dxdy + \int\int_{G-F}(||x||+||y||)dxdy\right]$$
$$= \frac{1}{N^2}\left[\int\int_F g(m)dxdy + \int\int_G (||x||+||y||)dxdy\right]$$
$$= \frac{g(m)}{N^2}\int\int_F dxdy + S_0^{\mathrm{TGS}}$$
$$= 2\Re + S_0^{\mathrm{TGS}}. \tag{18}$$

https://doi.org/10.1017/S0263574714000903 Published online by Cambridge University Press

Case 2

When one shadow area is within another local basin's shadow area, i.e. $F_1 \cup F_2 = F_1$ as in Fig. 7(b), the cost can be written as 19,

$$\begin{aligned} S_{2.2}^{\mathrm{TGS}} &\approx \frac{1}{N^2}\left[\int\int_{F_1-F_2}(||x||+||y||+g(m))dxdy+\int\int_{F_2}(||x||+||y||+2\times g(m))dxdy\right] \\ &\quad +\int\int_{SF-F_1-F_2}(||x||+||y||)dxdy\Bigg] \\ &= \frac{1}{N^2}\left[\int\int_{F_1} g(m)dxdy+\int\int_{F_2} g(m)dxdy+\int\int_{SF}(||x||+||y||)dxdy\right] \\ &= \frac{1}{N^2}\left[\int\int_{F_1} g(m)dxdy+\int\int_{F_2} g(m)dxdy\right]+S_0^{\mathrm{TGS}}. \end{aligned} \tag{19}$$

Since local basins are randomly placed, (19) also equals $2\Re + S_0^{\mathrm{TGS}}$. As a result, the expected travel cost with two local basins can be obtained as $S_2^{\mathrm{TGS}} \approx 2\Re + S_0^{\mathrm{TGS}}$.

3.3.3. Cost with k local basins. When k local basins are presented in a searching space, the expected cost is denoted as S_k^{TGS}. Considering (16) and (19), a hypothesis that $S_k^{\mathrm{TGS}} \approx k\Re + S_0^{\mathrm{TGS}}$ is established. Using mathematical induction, it is assumed that $S_{k-1}^{\mathrm{TGS}} = (k-1)\Re + S_0^{\mathrm{TGS}}$. Thus, the case with k local basins can be considered as adding the kth local basin to a searching space with $k-1$ local basins. The adding of the kth local basin has four different cases. First, F_k is not overlapped with any existing shadow areas, which is similar to Case 1 in Section 3.2.2. Second, F_k is inside at least one existing shadow area, this case is the same as Case 2 in Section 3.2.2. Third, F_k covers one or more other shadow areas. It is also similar to Case 2 in Section 3.2.2). Fourth is the union of the previous two cases. Again, it is similar to the second case in Section 32.2. Here the last case is discussed as an example.

As shown in Fig. 7(c), the kth local basin is added to the searching space with $k-1$ local basins. It is assumed that F_k is covered by i existing shadow areas and covers j existing shadow areas. For convenience, the j existing local basins are renumbered from bottom to top as 1st, 2nd ... jth. The difference between the costs before and after adding the kth local basin is:

$$\begin{aligned} S_k^{\mathrm{TGS}} - S_{k-1}^{\mathrm{TGS}} \approx \frac{1}{N^2}\Bigg[&\int\int_{F_K-F_1} g(m)dxdy+\int\int_{F_1-F_2} 2g(m)dxdy \\ &\ldots+\int\int_{F_{(j-1)}-F_j} jg(m)dxdy+\int\int_{F_J}(j+1)g(m)dxdy \\ &-\int\int_{F_1-F_2} g(m)dxdy-\int\int_{F_2-F_3} 2g(m)dxdy \\ &\ldots-\int\int_{F_{(j-1)}-F_j}(j-1)g(m)dxdy-+\int\int_{F_j} jg(m)dxdy\Bigg] \end{aligned}$$

https://doi.org/10.1017/S0263574714000903 Published online by Cambridge University Press

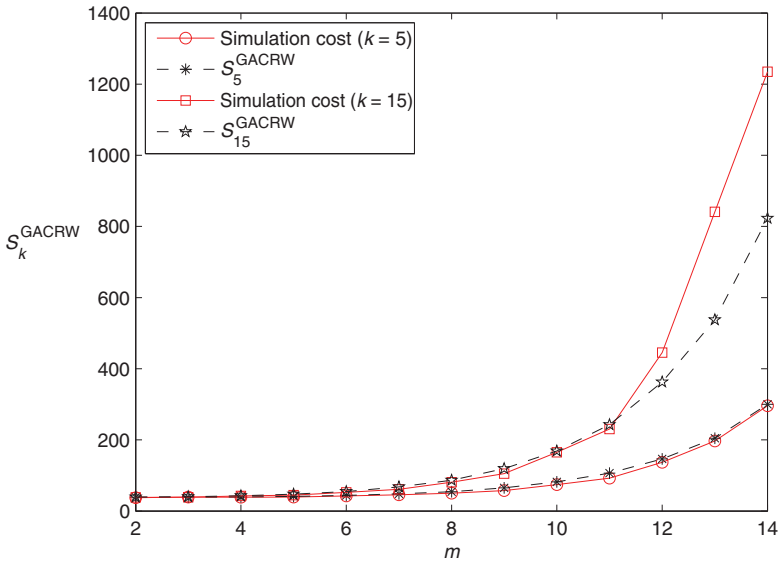


Fig. 8. Travel cost versus local basin size m in GACRW ($N = 100$).

$$= \frac{1}{N^2}\left[\int\int_{F_k} g(m)dxdy\right]$$
$$= \Re. \tag{20}$$

Thus, the average cost of TGS with k local basins can be written as $k\Re + S_0^{TGS}$. If we use $g(m) = m^2$ as the cost of escaping a single local basin, the cost of search in a searching space with k local basins can be obtained using Eqs. (15), (17), and (20),

$$S_k^{TGS} \approx k\Re + S_0^{TGS}$$
$$= \frac{12N^4 + km^3(8N^2 - 10m^2 + 43mN)}{24N^3}. \tag{21}$$

Since the virtual wall problem is unlikely to occur in a sparse local basin, the obtained S_k^{TGS} in (21) is lower than the true cost. Although the virtual wall problem is inevitable in TGS, S_k^{TGS} is a good approximation of true cost, especially when local basins are sparse.

4. Simulation and Results

4.1. Comparison of analytical cost and simulation cost

4.1.1. Gradient ascent with correlated random walk. The derived S_k^{GACRW} is compared with the cost obtained from numerical simulations. For each set of N, m, and k, 1000 trials are taken in simulation. A robot starts from a random point and is regarded as arriving at the target when the global maximum point is within one step.

Figure 8 illustrates the analytical cost compared with those obtained from simulations in different parameter settings. Under a fixed searching space size $N = 100$, the analytical cost well predicts the cost in simulation, especially when k is small.

The S_k^{GACRW} matches well with the simulation cost in Fig. 9. The results demonstrate that S_k^{GACRW} can adequately represent a good prediction of numerical simulation in regions where m and k are not large. Also, it is obvious that S_k^{GACRW} increases linearly with the growth of k. Note the gap between

https://doi.org/10.1017/S0263574714000903 Published online by Cambridge University Press

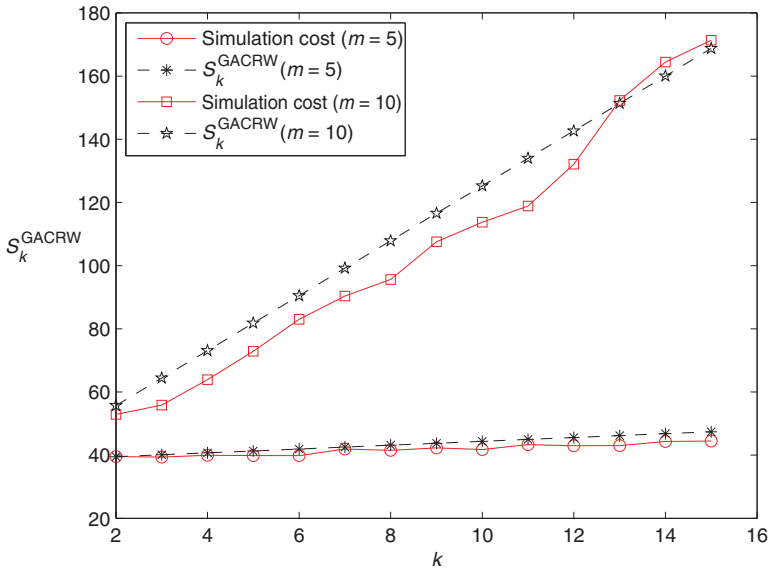


Fig. 9. Travel cost versus local basin number k in GACRW (N= 100).

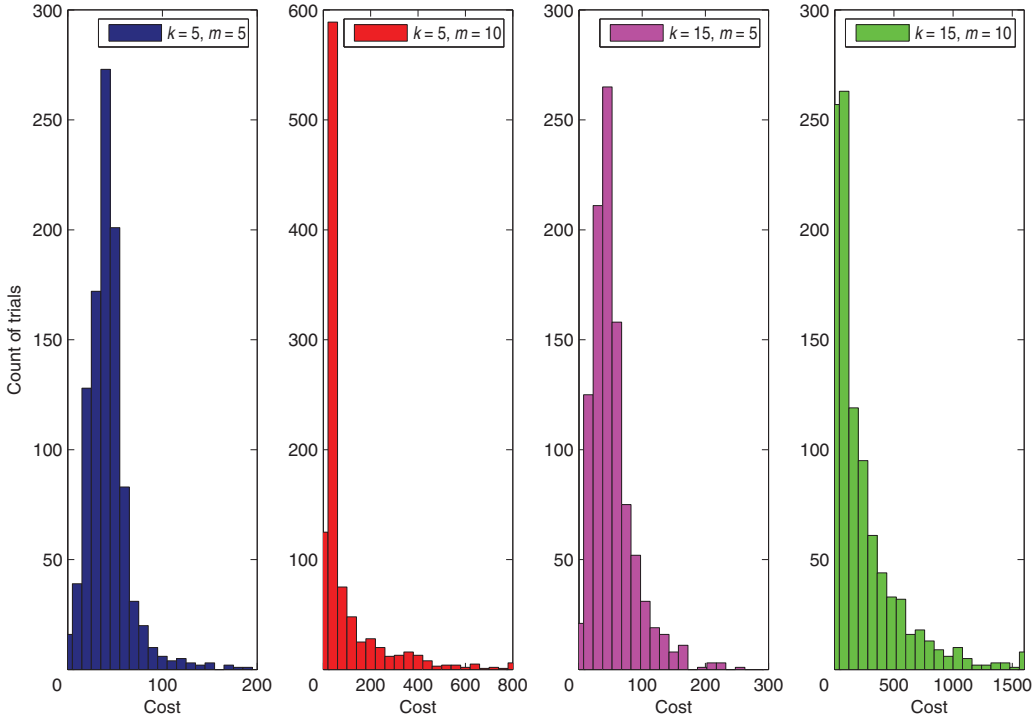


Fig. 10. Histogram of travel cost in GACRW (N=100). The distributions of travel costs are under different m and k pairs for each 1000 trials.

S_k^{GACRW} and the simulation cost arise because the approximation in deriving S_k^{GACRW} is less accurate when m is large, as we mentioned in (b) in Section 3.2.1.

In Fig. 10 the histograms reveal the same trend that the travel cost increases together with m and k.

4.1.2. Theseus gradient search. The derived S_k^{TGS} is also compared with the cost obtained from numerical simulations. Similarly, 1000 trials are taken in simulation. Figure 11 presents a typical

https://doi.org/10.1017/S0263574714000903 Published online by Cambridge University Press

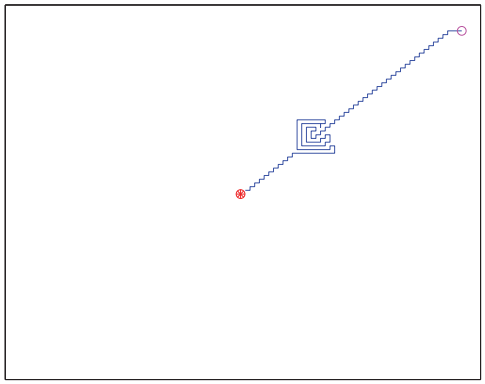


Fig. 11. A typical trajectory of TGS on a gradient field with local basins (N = 100, m = 8).

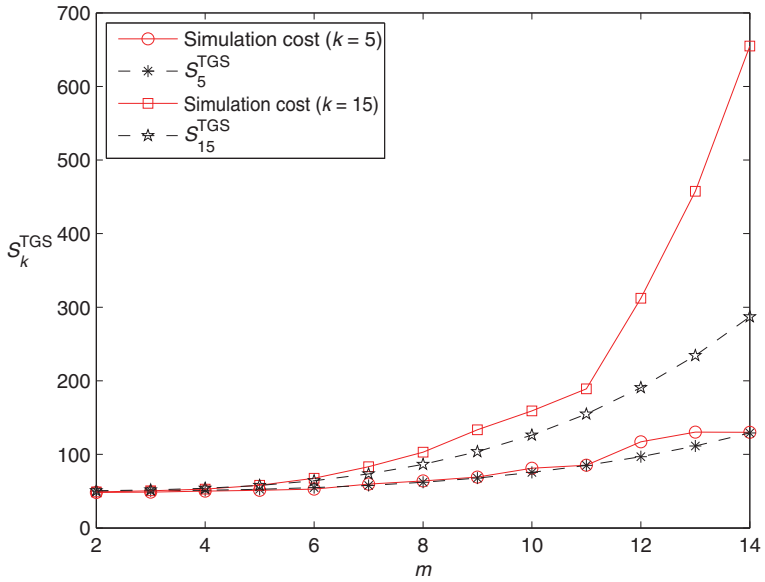


Fig. 12. Travel cost versus local basin size m in TGS (N=100).

trajectory in simulation where a robot starts from the top right position targeting at the red global peak. While searching, the robot uses self-avoidance walk to escape the local basin.

In Fig. 12, the curve of S_5^{TGS} matches well with the cost obtained from simulation. When $k = 15$, S_{15}^{TGS} is slightly higher than the cost from simulation as $m \leq 11$.

In Fig. 13, when $m = 5$, S_k^{TGS} coincides with the cost from simulation. When $m = 10$, although not perfectly matched, S_k^{TGS} provides a good prediction on the true cost. In both Figs. 12 and 13, the difference between S_k^{TGS} and the cost obtained from simulations is mainly caused by the virtual walls which are not taken into consideration in the analysis.

In Fig. 14, a set of histograms similar to Fig. 10 are presented.

4.2. Comparison between the analytical costs

A few interesting properties of GACRW and TGS can be observed by comparing their analytical costs as shown in Fig. 15. When m is small ($k = 5$, $m < 9$; $k = 15$, $m < 7$), the cost of TGS is slightly higher than that of GACRW. This is due to the fact that S_0^{GACRW} is lower than S_0^{TGS} as from Eqs. (11) and (15) respectively. As the local basins become denser, S_k^{GACRW} grows much faster than S_k^{TGS}. More importantly, after the critical point where S_k^{TGS} becomes lower than S_k^{GACRW}, the gap between their costs increases exponentially with the growth of m.

https://doi.org/10.1017/S0263574714000903 Published online by Cambridge University Press

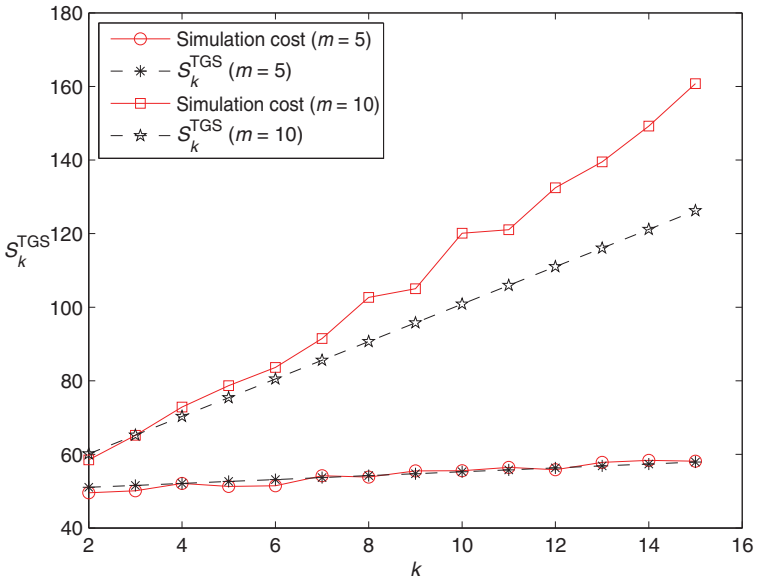


Fig. 13. Travel cost versus local basin number k in TGS (N=100).

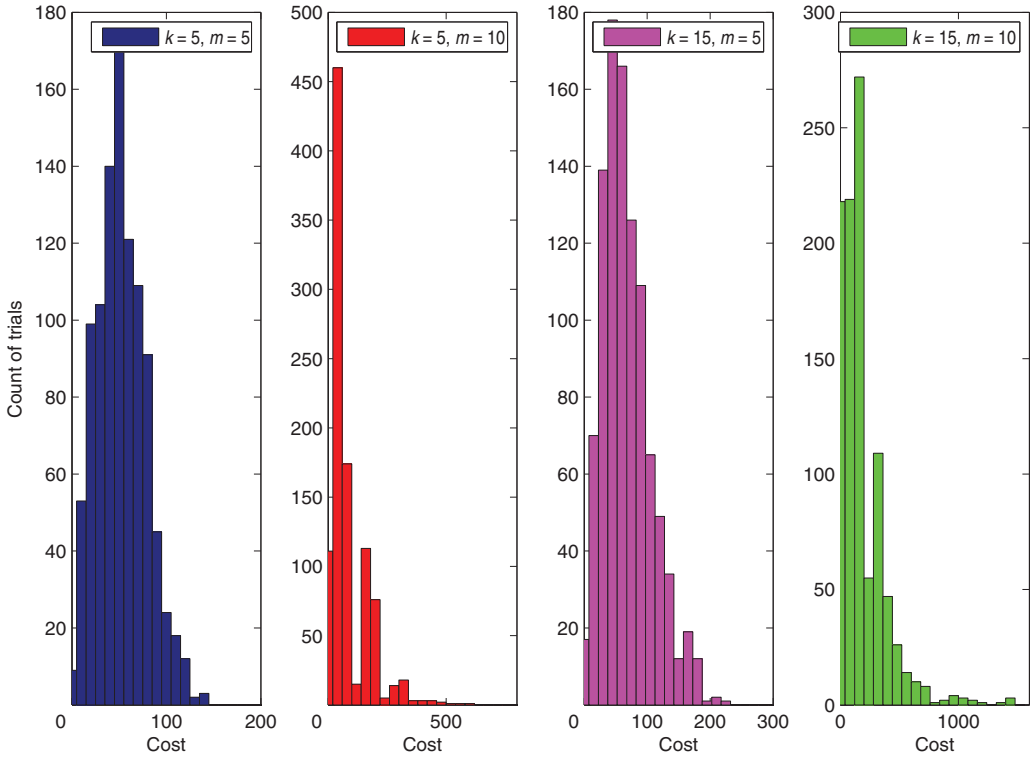


Fig. 14. Histogram of travel cost in TGS (N=100). The distributions of travel costs are under different m and k pairs for each of 1000 trials.

4.3. Simulation comparison in the gradient field

The four algorithms are compared in terms of cost in the gradient field by simulation: TGS, GACRW, E. coli algorithm (E coli),[2, 12, 26] and chemotaxis (Chem).[20] We slightly modify the criteria of behavior switches in E. coli and Chem to fit the gradient field: As soon as the inner product of the latest motion and the current gradient becomes negative, a behavior switch is triggered. We regard this as equivalent to the conditions in E. coli and Chem of $C = 0$. Also, ε_θ is chosen as $\frac{\pi}{2}$ in Chem.[20] With each set of N, m, and k, 1000 trials are taken into simulation for each algorithm.

https://doi.org/10.1017/S0263574714000903 Published online by Cambridge University Press

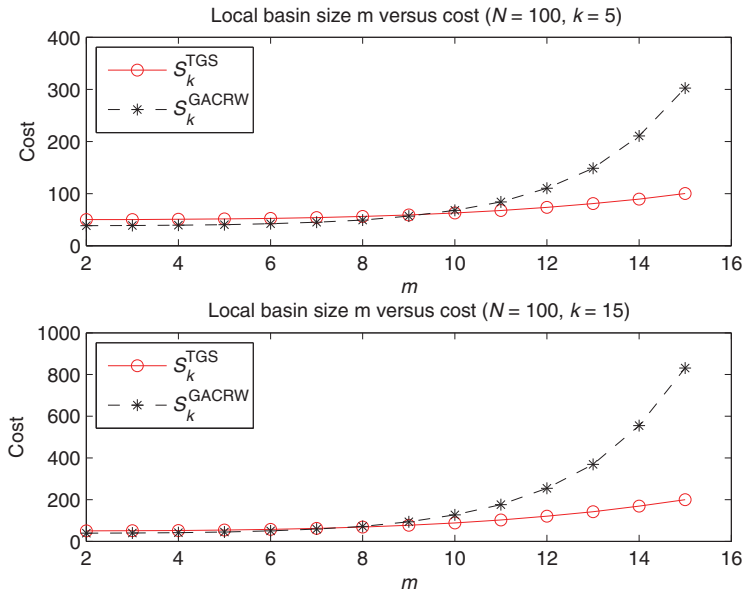


Fig. 15. Analytical cost versus local basin size m.

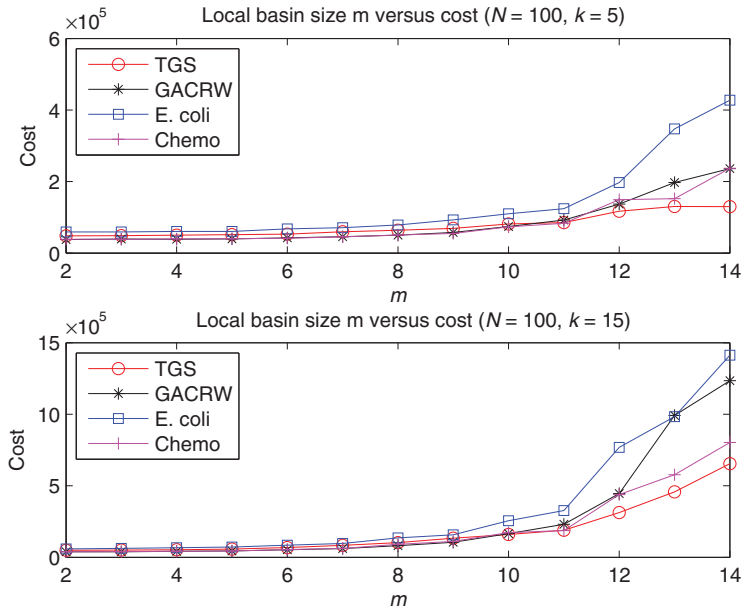


Fig. 16. Travel cost versus local basin size m.

Figure 16 shows that when $m \geq 11$, TGS has the lowest cost out of the four. On the other hand, TGS costs slightly higher than others for small m. This result is intuitively understandable since TGS is designed in the taxicab geometry and its cost is the highest out of the four if there is no local basin. Fortunately, local basins dominate the cost in practical applications. Thus, it is reasonable to see that TGS costs the lowest where m becomes larger.

4.4. Simulation comparison with real data

The above comparisons are all performed in gradient fields that highlight the local basins but ignore the noisy gradients. In this section, we compare the four algorithms in a radio source search using RSS in a hallway. To validate the results in high fidelity, the simulation is driven by real data. As shown in Fig. 2, four radio sources are placed at A, B, C, and D. The hallway is partitioned into 343 grids of size 1×1 square feet (0.3048×0.3048 square meters). At the center of each grid, 10 readings for each

https://doi.org/10.1017/S0263574714000903 Published online by Cambridge University Press

Table I. Average cost in search (meters).

Targets	A	B	C	D
TGS	29.3	52.5	51.4	36.9
GACRW	44.0	98.8	104.5	89.2
E. coli	56.0	235.4	271.7	109.6
Chem	54.9	194.2	248.0	90.5

radio source are collected using the micaz sensor node. Interpolations are performed to smooth the RSS distribution. Both local basins and noisy gradients are presented in this practical scenario since the RSS distribution is highly rugged due to multi-path effect. A contour map of RSS distribution for radio source A is shown in Fig. 2.

At each trial, a robot starting from a random point is sent to find one assigned radio source using RSS. Noting that empirical behavior-based algorithms, such as Hex-Path,[27] is likely to fail in such a practical scenario. In the simulation, the step length is 0.6096 meters. Major parameters in Chem are $C = 0$, $\varepsilon_\theta = \frac{\pi}{2}$. A target radio source will be regarded as found when the distance between the robot and the target is smaller than 0.6096 meters. For each algorithm, 200 simulation trials are launched for each radio source.

The results in Table I further confirm the applicability and reliability of TGS and GACRW. The costs of TGS are always lower than others, while costs of GACRW are lower than E. coli and Chem. The main reason is that TGS and GACRW are robust to the noisy environments, while the chemotaxis-based methods are not. Furthermore, TGS is less influenced by the local basins than GACRW, especially when local basins are dense. Considering these facts, the result is not surprising. Also, the costs for different sources are significantly different. For example, TGS takes 29.3 meters on average for source A, while 51.4 meters for source C. This is because radio source C covers more areas than A. In other words, the searching space for source C is larger than that for source A. Although a larger searching space always yields a higher cost, the range of cost growth differs. Specifically, using TGS, the cost for C is 0.77 times higher than that for A. While using E. coli, the cost for C is 3.8 times higher than that for A. In the table, TGS has the lowest cost growth range, while GACRW has the second lowest. It indicates that TGS and GACRW are more flexible and robust compared with the chemotaxis-based algorithms.

Another point worthy to mention is that the performance of the four algorithms varies with parameter settings. However, the order of cost does not change significantly. Specifically, if the step length is reduced, the costs in all four algorithms will grow since reducing step length is equivalent to raising sizes of both local basins and searching space. This is related to the problem if the performance of the algorithms is scalable to the physical step length. Even then the cost of TGS grows the slowest among the four algorithms.

5. Conclusions

In this paper, we have applied GACRW in source search, and proposed TGS in the same context. The proposed TGS takes advantage of the well-known dead reckoning to exhaust and escape the local basins in short periods, and exploits the gradients to approach the global peak. Compared with the class of chemotaxis algorithms, both TGS and GACRW allow the robot to escape local basins faster. We have analytically investigated both algorithms in the gradient field with local basins. The travel cost for each algorithm in a gradient field was derived, and then confirmed by numerical simulations. To the best of our knowledge, this work is the first to propose the gradient field that enables the analysis of source searching algorithms. By comparing the costs of GACRW and TGS in the gradient field, it is shown that TGS is more flexible and robust to local basins, and costs less except in the cases where local basins are sparse. The comparisons among costs of GACRW, TGS, E.coli, and Chem reveal that GACRW and TGS outperform the chemotaxis-based algorithms since the former two are tolerant with noisy gradients. In our future works, we will propose and analyze the searching algorithms in more general gradient fields, and perform the corresponding field verifications using mobile robots.

https://doi.org/10.1017/S0263574714000903 Published online by Cambridge University Press

References

1. J. Adler, "Chemotaxis in bacteria," *Science* **153**(3737), 708–716 (1966).
2. J. Adler, "The sensing of chemicals by bacteria," *Sci. Am.* **234**(4), 40–47 (1976).
3. J. Atema, "Eddy chemotaxis and odor landscapes: Exploration of nature with animal sensors," *Biol. Bull.* **191**, 129–139 (Aug. 1996).
4. H. C. Berg, *E. Coli in Motion* (Springer, Berlin, Germany, 2004).
5. J. A. Byers, "Correlated random walk equations of animal dispersal resolved by simulation," *Ecology* **82**(6), 1680–1690 (Jun. 2001).
6. E. K. P. Chong and S. H. Zak, *An Introduction to Optimization*, 2nd ed. (Wiley-Interscience, River Street Hoboken, NJ, 2001).
7. E. A. Codling, M. J. Plank and S. Benhamou, "Random walk models in biology," *J. R. Soc. Interface* **5**(25), 813–834 (Aug. 2008).
8. R. Cowlagi and P. Tsiotras, "Multiresolution motion planning for autonomous agents via wavelet-based cell decompositions," *IEEE Trans. Syst. Man Cybern.* **42**(5), 1455–1469 (Oct. 2012).
9. E. H. Lloyd, "What is, and what is not, a Markov chain?," *J. Hydrol.* **22**(1–2), 1–28 (1974).
10. G. S. Fraenkel and D. L. Gunn, *The Orientation of Animals: Kineses, Taxes and Compass Reactions* (Dover, Kent, UK, 1961).
11. C. M. Grinstead and L. J. Snell, *Introduction to Probability* (American Mathematical Society, Providence, RI, 2006).
12. O. Holland and C. Melhuish, "Some Adaptive Movements of Animats with Single Symmetrical Sensors," **In**: *From Animals to Animats*, (P. Maes, M. Mataric, J. Meyer, J. Pollack and S. Wilson, eds) vol. 4 (MIT Press, Cambridge, UK, 1996) pp. 55–64.
13. H. Ishida, K. Suetsugu, T. Nakamoto and T. Moriizumi, "Study of autonomous mobile sensing system for localization of odor source using gas sensors and anemometric sensors," *Sensors Actuators A* **45**(2), 153–157 (1994).
14. X. Jin and A. Ray, "Coverage Control of Autonomous Vehicles for Oil Spill Cleaning in Dynamic and Uncertain Environments," *American Control Conference (ACC), 2013*, Washington, DC, USA. (Jun. 2013) pp. 2594–2599.
15. X. Jin and A. Ray, "Navigation of autonomous vehicles for oil spill cleaning in dynamic and uncertain environments," *Int. J. Control*, **87**(4), 1–15 (2014).
16. D. S. Johnson, J. M. London, Lea, M.-A. and J. W. Durban, "Continuous-time correlated random walk model for animal telemetry data," *Ecology* **89**(5), 1208–1215 (May 2008).
17. P. M. Kareiva and N. Shigesada, "Analyzing insect movement as a correlated random walk," *Oecologia* **56**, 234–238 (1983).
18. G. Kowadlo and R. A. Russell, "Robot odor localization: A taxonomy and survey," *Int. J. Robot. Res.* **27**(8), 869–894 (2008).
19. L. Marques, U. Nunes and A. T. de Almeida, "Olfaction-based mobile robot navigation," *Thin Solid Films* **418**(1), 51–58 (2002).
20. S. G. Nurzaman, Y. Matsumoto, Y. Nakamura, S. Koizumi and H. Ishiguro, "Yuragi-Based Adaptive Searching Behavior in Mobile Robot: From Bacterial Chemotaxis to Levy Walk," *IEEE International Conference on Robotics and Biomimetics, 2008*, Bangkok, Thailand. (22–25 Feb. 2009) pp. 806–811.
21. W. Park, Y. Liu, Y. Zhou, M. Moses and G. S. Chirikjian, "Kinematic state estimation and motion planning for stochastic nonholonomic systems using the exponential map," *Robotica* **26**(4), 419–434 (2008).
22. C. S. Patlak, "A mathematical contribution to the study of orientation of organisms," *Bull. Math. Biophys.* **15**(4) (1953), 431–476.
23. C. S. Patlak, "Random walk with persistence and external bias," *Bull. Math. Biophys.* **15**(3), 311–338 (1953).
24. K. Pearson, "The problem of the random walk," *Nature* **72**(1865), 294 (1905).
25. B. Porat and A. Nehorai, "Localizing vapor-emitting sources by moving sensors," *IEEE Trans. Signal Process.* **44**(4), 1018–1021 (1996).
26. R. Russell, B.-A. Hadiashar, R. L. Shepherd and G. G. Wallace, "A comparison of reactive robot chemotaxis algorithms," *Robot. Auton. Syst.* **45**(2), 83–97 (2003).
27. R. A. Russell, "Robotic location of underground chemical sources," *Robotica* **22**(1), 109–115 (2004).
28. R. A. Russell, D. Thiel, R. Deveza and A. Mackay-sim, "A Robotic System to Locate Hazardous Chemical Leaks," *Proceedings of the IEEE International Conference on Robotics and Automation*, Nagoya, Japan. (21-27 May 1995), pp. 556–561.
29. D. W. Sims, E. J. Southall, N. E. Humphries, G. C. Hays, C. J. A. Bradshaw, J. W. Pitchford, A. James, M. Z. Ahmed, A. S. Brierley, M. A. Hindell, D. Morritt, M. K. Musyl, D. Righton, E. L. C. Shepard, V. J. Wearmouth, R. P. Wilson, M. J. Witt, and J. D. Metcalfe, "Scaling laws of marine predator search behaviour," *Nature* **451**(7182), 1098–1102 (Feb. 2008).
30. D. Song, C.-Y. Kim and J. Yi, "Monte Carlo Simultaneous Localization of Multiple Unknown Transient Radio Sources Using a Mobile Robot with a Directional Antenna," *IEEE International Conference on Robotics and Automation, 2009*, New York City, NY, USA. (Dec. 17, 2009) pp. 3154 –3159.
31. D. Song, J. Yi and Z. Goodwin, "Localization of Unknown Networked Radio Sources Using a Mobile Robot with a Directional Antenna," *American Control Conference, 2007 (ACC '07)* (Sep. 13, 2007) pp. 5952–5957.

https://doi.org/10.1017/S0263574714000903 Published online by Cambridge University Press

32. Y. Sun, J. Xiao, X. Li and F. Cabrera-Mora, "Adaptive Source Localization by a Mobile Robot Using Signal Power Gradient in Sensor Networks," *Global Telecommunications Conference, 2008*, New Orleans, LA, USA. (Nov. 2008) pp. 1–5.
33. M. Vergassola, E. Villermaux and B. I. Shraiman, "Infotaxis as a strategy for searching without gradients," *Nature* **445**(7126), 406–409 (2007).
34. G. Viswanathan, E. Raposo and M. da Luz "Levy flights and superdiffusion in the context of biological encounters and random searches," *Phys. Life Rev.* **5**(3), 133–150 (2008).
35. F. W Grasso, T. R. Consi, D. C. Mountain and J. Atema, "Biomimetic robot lobster performs chemo-orientation in turbulence using a pair of spatially separated sensors: Progress and challenges," *Robot. Auton. Syst.* **30**(1–2), 115–131 (2000).
36. X. Zhang, Y. Sun and J. Xiao, "Radio Source Search Using Force Field Vectors Weighted by Received Signal Strength Gradients," *2011 International Conference on Mechatronics and Automation (ICMA)*, Beijing, China (7–10 Aug. 2011) pp. 531–536.
37. X. Zhang, Y. Sun and J. Xiao, "A novel radio source search algorithm using force field vectors and received signal strengths," *Int. J. Mechatronics Autom.* **3**(1), 25–35 (2013).
38. X. Zhang, Y. Sun, J. Xiao and F. Cabrera-Mora, "Theseus Gradient Guide: An Indoor Transmitter Searching Approach Using Received Signal Strength," *IEEE International Conference on Robotics and Automation, 2011*, Shanghai, China (May 2011) pp. 2560–2565.

https://doi.org/10.1017/S0263574714000903 Published online by Cambridge University Press